DNA specificity enhanced by sequential binding of protein monomers

Jennifer J. Kohler*, Steven J. Metallo*, Tanya L. Schneider, and Alanna Schepartz†

Department of Chemistry, Yale University, New Haven, CT 06511

Communicated by Paul B. Sigler, Yale University, New Haven, CT, August 5, 1999 (received for review May 15, 1999)

Transcriptional activation often requires the rapid assembly of complexes between dimeric transcription factors and specific DNA sites. Here we show that members of the basic region leucine zipper and basic region helix–loop–helix zipper transcription factor families follow an assembly pathway in which two protein monomers bind DNA sequentially and form their dimerization interface while bound to DNA. Nonspecific protein or DNA competitors have little effect on the rate of assembly along this pathway, but slow a competing pathway in which preformed dimers bind DNA. The sequential monomer-binding pathway allows the protein to search for and locate a specific DNA site more quickly, resulting in greater specificity prior to equilibrium.

Activation of transcription requires the formation of large, multicomponent protein–DNA complexes (1). These complexes choose their route of assembly from many potential pathways. *In vivo*, the pathway chosen will depend on the availability of components and the relative rate constants of individual steps along each pathway, as well as on the propensities of intermediates to engage in alternative interactions with other nuclear components (2). Some of these alternative interactions can be nonproductive or even detrimental, whereas others might allow productive retargeting of a transcription factor in response to cellular stimuli.

Many transcription factors bind DNA to form dimeric (2:1) protein–DNA complexes. Examples include basic region leucine zipper (bZIP) proteins and basic region helix–loop–helix zipper (bHLHZip) proteins. For these proteins, there exist two limiting pathways that may describe the route of complex assembly (Fig. 1). The protein can dimerize first, then associate with DNA (dimer pathway), or can follow a pathway in which two monomers bind DNA sequentially and assemble their dimerization interface while bound to DNA (monomer pathway) (3–10). Because these transcription factors (or their derivatives) often have been observed in dimeric form in the absence of DNA, complex assembly has been assumed to proceed via the dimer pathway. Here we show that, for members of the bZIP and bHLHZip families, the rate of DNA binding is rapid and cannot be accounted for by assembly through the dimer pathway. For these proteins, we propose that DNA binding occurs via the monomer pathway. Furthermore, we show that excess nonspecific protein or DNA competitors, even at low concentrations, slow the dimer pathway but not the monomer pathway. By minimizing apportionment of a transcription factor into incorrect, nonspecific complexes prior to equilibrium, the monomer pathway allows for rapid identification of a specific DNA site in response to cellular stimuli. Therefore, not only does the monomer pathway allow for faster assembly of certain bZIP and bHLHZip transcription factor dimer–DNA complexes, it also provides an efficient means of discriminating between specific and nonspecific DNA target sites. This method of kinetic discrimination has implications for the regulation of transcription by both cellular and viral proteins.

Materials and Methods

Peptides and DNA. Activating transcription factor 2 $(ATF\text{-}2)_{350–505}$ (ref. 11) and $Max_{22–113}$ (ref. 12) have been reported. $Max^{SH}_{22–105}$ (ref. 12) contained residues 22–105 of Max with the amino acid sequence Gly-Gly-Cys-Asp appended to the C terminus. $Max^{SFlu}_{22–105}$ was produced by alkylation of the unique cysteine in $Max^{SH}_{22–105}$ with 5-iodoacetamidofluorescein (Molecular Probes) and was purified by reverse-phase HPLC. $Max^{SS}_{22–105}$ was produced by oxidation of $Max^{SH}_{22–105}$ and was purified by reverse-phase HPLC. DNA sequences employed were as follows: CRE_{24}, d(AGTGGAGATGACGTCATCTCGTGC), $Ebox_{22}$, d(GTGTAGGCCACGTGACCGGGTG), and $hsEbox_{22}$, d(GTGTAGGCCTAGTGACCGGGTG).

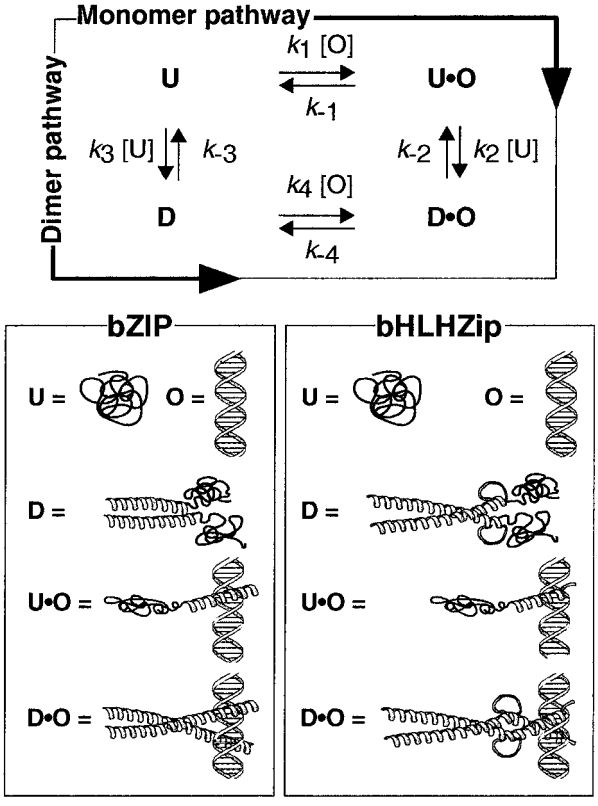

Fig. 1. Two pathways for binding bZIP and bHLHZip proteins to DNA.

CD Experiments. Equilibrium CD spectra were acquired at 25°C on an Aviv 62DS spectrophotometer, and ellipticity at 222 nm was plotted as a function of protein concentration. Each data point

Abbreviations: bZip, basic region leucine zipper; bHLHZip, basic region helix–loop–helix zipper; ATF-2, activating transcription factor 2.

*J.J.K. and S.J.M. contributed equally to this work.

†To whom reprint requests should be addressed. E-mail: alanna.schepartz@yale.edu.

The publication costs of this article were defrayed in part by page charge payment. This article must therefore be hereby marked "*advertisement*" in accordance with 18 U.S.C. §1734 solely to indicate this fact.

represented the average of three independent trials. The data were fit to the equation (13): $2M_0f_m^2 + f_mK_{dim} - K_{dim} = 0$, where M_0 = $[protein]_{Total}$, K_{dim} = the equilibrium dissociation constant of the protein dimer, and f_m = the fraction of the total CD signal observed $[(\Theta_{observed} - \Theta_{max})/(\Theta_{min} - \Theta_{max})]$. For both ATF-$2_{350-505}$ and Max_{22-113}, equivalent K_{dim} values were also determined by fluorescence polarization. ATF-$2_{350-505}$ CD spectra were acquired in 1× PBS (1.4 mM KH_2PO_4/4.3 mM Na_2HPO_4/2.7 mM KCl/137 mM NaCl, pH 7.4) containing 1 mM DTT. Max_{22-113} spectra were acquired in 1× PBS. CD experiments performed in the presence of 1× PBS containing 5% glycerol and 1 mM EDTA demonstrated that these two components did not increase the amount of α-helical structure within Max_{22-113}.

To monitor the Max_{22-113} monomer–dimer transition by CD, a solution of $[Max_{22-113}]_{Total}$ = 50 μM was diluted 50-fold into PBS buffer at 25°C and the negative ellipticity at 222 nm was monitored as a function of time. Each point was averaged over 20 sec and corrected for the signal arising from buffer.

Stopped-Flow Fluorescence. To monitor the kinetics of the ATF-$2_{350-505}$ monomer–dimer transition, a solution of ATF-$2_{350-505}$ in 1× PBS containing 1 mM DTT was diluted 10-fold and the intrinsic tryptophan fluorescence was monitored as a function of time. Each point represented the average of data accumulated over 0.2 sec. Kinetic traces were acquired at 25°C on a KinTek SF-2001 stopped-flow spectrophotometer with an excitation wavelength of 280 nm, and emission was monitored at 340 nm with a 12-nm bandpass filter (Corion, Holliston, MA). Relaxation rates ($1/\tau$) were determined from the fit to a single exponential and represented the average of at least 50 independent experiments at each concentration between 10 and 30 μM ATF-$2_{350-505}$. Data were fit to the linearized rate equation $1/\tau = 4k_3(\text{ATF-}2_{350-505})_{monomer} + k_{-3}$ (14) to determine k_3 and k_{-3}.

To monitor $[\text{ATF-}2_{350-505}]_2$·$CRE_{24}$ association kinetics, a 200-nM solution of ATF-$2_{350-505}$ was mixed rapidly with 100 nM CRE_{24} and the fluorescence was monitored as a function of time. Each point represented the average of data accumulated over 0.2 sec. The relaxation rate ($1/\tau$) was determined from the fit to a single exponential and represented the average of 50 independent experiments. Simulations of the monomer and dimer pathways were performed by using KINTEKSIM software (15). The starting dimer concentration used to simulate the dimer pathway was defined by either k_{-3}/k_3 or K_{dim}.

Stopped-Flow Polarization. A solution of 5 μM Max^{SFlu}_{22-105} was diluted 10-fold into 1× PBS at 25°C, and the fluorescence anisotropy was monitored as a function of time (16). Each point represented the average of data accumulated over 0.5 sec.

Electrophoretic Mobility-Shift Experiments. Max_{22-113} was incubated in binding buffer (1× PBS containing 0.1% Nonidet P-40, 400 μg/ml BSA, 5% glycerol, and 1 mM EDTA) for 30 min at 25°C. [^{32}P]$Ebox_{22}$ was added to a concentration of 50 pM, and the reaction was followed by loading aliquots on a nondenaturing 8% (49:1) polyacrylamide gel. Radioactivity was quantified by using a STORM 840 PhosphorImager (Molecular Dynamics). Simulations of the monomer and dimer pathways were performed by using KINTEKSIM software (15). For experiments comparing the rate of binding through the monomer and dimer pathways, a mixture of 8 nM Max_{22-113} and 1.9 nM Max^{SS}_{22-105} was incubated for 30 min at 25°C in binding buffer in the absence or presence of 10 nM $hsEbox_{22}$. To each reaction was added 2 nM [^{32}P]$Ebox_{22}$, and the partitioning of [^{32}P]$Ebox_{22}$ into complexes with Max_{22-113} and Max^{SS}_{22-105} was monitored as a function of time. The reactions were followed by electrophoresis as described above. Analogous experiments were performed with either 0.57 μg/ml calf thymus DNA or 22.7 μg/ml HeLa cell nuclear extracts (Promega) as the competitor.

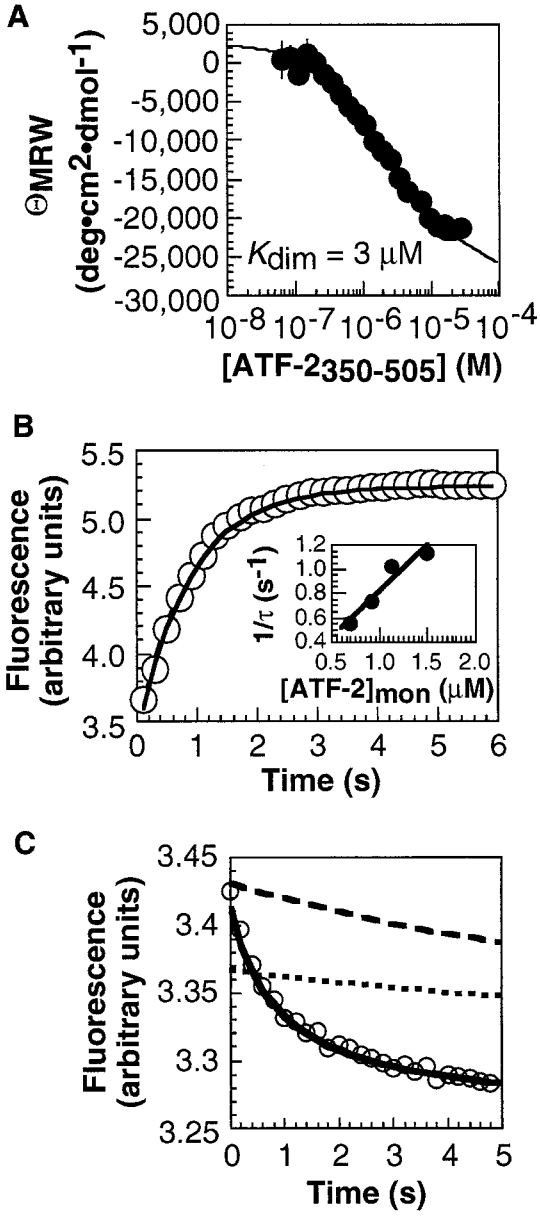

Fig. 2. Analysis of ATF-$2_{350-505}$ monomer–dimer equilibrium and kinetics and $[\text{ATF-}2_{350-505}]_2$·$CRE_{24}$ association kinetics. (*A*) ATF-$2_{350-505}$ monomer–dimer equilibrium analyzed by CD. (B) ATF-$2_{350-505}$ monomer–dimer kinetics analyzed by stopped-flow fluorescence spectroscopy. A solution of $[\text{ATF-}2_{350-505}]_{Total}$ = 30 μM was diluted 10-fold, and the fluorescence was monitored as a function of time. (*Inset*) Relaxation rate as a function of $[\text{ATF-}2_{350-505}]_{monomer}$. (*C*) $[\text{ATF-}2_{350-505}]_2$·$CRE_{24}$ association kinetics analyzed by stopped-flow fluorescence spectroscopy. A 200-nM solution of ATF-$2_{350-505}$ was mixed rapidly with 100 nM CRE_{24}, and the fluorescence was monitored as a function of time. The relaxation rate ($1/\tau$) was determined from the fit to a single exponential. Simulations of binding of CRE_{24} by ATF-$2_{350-505}$ via the monomer (solid line) and dimer pathways are shown. The concentration of $[\text{ATF-}2_{350-505}]_2$ at the start of the simulation along the dimer pathway was defined either by the ratio k_{-3}/k_3 determined by fluorescence (dotted line) or by K_{dim} determined by equilibrium CD measurements (dashed line). In neither case can the dimer pathway account for the rate of DNA binding.

Results and Discussion

The bZIP Protein ATF-$2_{350-505}$ Follows the Monomer Pathway to Bind DNA. Our previous studies showed that DNA binding by certain bZIP peptides (17) could not proceed through the dimer pathway; additional experiments provided evidence that the mono-

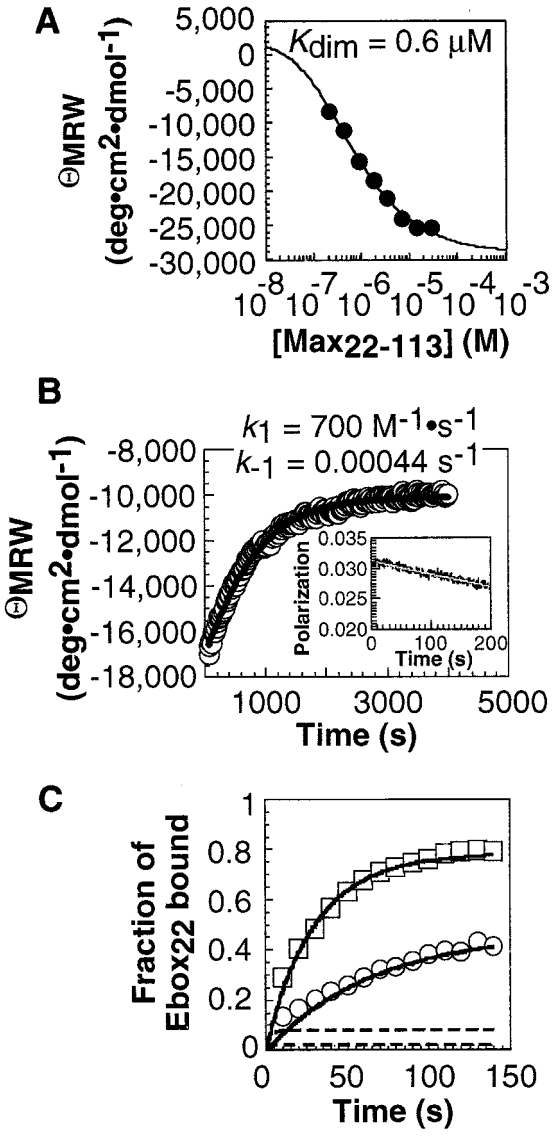

Fig. 3. Analysis of $Max_{22–113}$ monomer–dimer equilibrium and kinetics and $[Max_{22–113}]_2$·$Ebox_{22}$ association kinetics. (*A*) $Max_{22–113}$ monomer–dimer equilibrium analyzed by CD. (*B*) $Max_{22–113}$ monomer–dimer kinetics analyzed by CD and stopped-flow fluorescence. A 50-μM solution of $Max_{22–113}$ was diluted 50-fold into PBS buffer at 25°C, and the negative ellipticity at 222 nm was monitored as a function of time. (*Inset*) $Max^{SFlu}_{22–105}$ monomer–dimer relaxation kinetics monitored by stopped-flow fluorescence polarization within the first 200 sec of the reaction. A solution of 5 μM $Max^{SFlu}_{22–105}$ was diluted 10-fold into PBS buffer at 25°C, and the fluorescence anisotropy was monitored as a function of time. (*C*) Association of 1 nM (○) and 2 nM (□) $Max_{22–113}$ with 50 pM $Ebox_{22}$ at 25°C. Each point represented the average of at least three independent experiments. Error bars shown represent the SD. Similar association kinetics were observed with a 135-bp DNA fragment containing a single Ebox site (CACGTG). Simulations of binding of $Ebox_{22}$ by $Max_{22–113}$ via the monomer (solid lines) and dimer (dashed lines) pathways are shown.

mer pathway was followed (4). These bZIP element peptides formed coiled coils characterized by low thermodynamic stabilities. To evaluate whether a bZIP protein capable of forming a stable coiled coil would also follow the monomer pathway, we studied a 156-residue fragment of ATF-2 (ref. 18), ATF-$2_{350–505}$. The CD spectrum of ATF-$2_{350–505}$ was consistent with a fully helical dimerization region at concentrations greater than 10 μM (Fig. 2*A*). At lower concentrations, the ATF-$2_{350–505}$ dimer dissociated into unstructured monomers (K_{dim} = 3 μM) that were detected by an increase in ellipticity at 222 nm. The kinetics of the ATF-$2_{350–505}$ monomer–dimer transition were determined by using stopped-flow fluorescence spectroscopy. The ATF-$2_{350–505}$ dimer was formed at concentrations above 10 μM and diluted rapidly, and the intrinsic tryptophan fluorescence was monitored to determine the rate of relaxation from dimer to monomer (Fig. 2*B*). The time-dependent increase in fluorescence was fit to a single exponential to determine the relaxation rate, $1/\tau$, at each concentration. Association (k_3) and dissociation (k_{-3}) rate constants of 1.9×10^5 M^{-1}·s^{-1} and 0.05 s^{-1} were derived from a plot of $1/\tau$ vs. the concentration of ATF-$2_{350–505}$ monomer (14) (Fig. 2*B Inset*). The ratio k_{-3}/k_3 (0.3 μM) was comparable to the K_{dim} value determined in equilibrium experiments (3 μM).

To evaluate whether the ATF-$2_{350–505}$ dimer could function as an intermediate during formation of a specific DNA complex, we monitored association of ATF-$2_{350–505}$ with the oligonucleotide duplex CRE_{24} by stopped-flow fluorescence spectroscopy. Equilibrium measurements showed that the intrinsic fluorescence of ATF-$2_{350–505}$ diminished upon binding to CRE_{24} (data not shown). Kinetic experiments showed that binding of 200 nM ATF-$2_{350–505}$ and 100 nM CRE_{24} occurred rapidly; the time-dependent decrease in fluorescence was best described by a single exponential with a relaxation rate of 1 s^{-1} (Fig. 2*C*).

Binding of ATF-$2_{350–505}$ to CRE_{24} via the monomer and dimer pathways was simulated by using numerical integration (15). To simulate the dimer pathway, we employed experimentally determined values of k_3 (1.9×10^5 M^{-1}·s^{-1}) and k_{-3} (0.05 s^{-1}). The rate of DNA binding must be fast to account for the overall kinetics of the association reaction, so k_4 was set at 10^{10} M^{-1}·s^{-1}, a diffusion-limited second-order rate constant (19) that takes into account the potential influence of rate-enhancing parameters such as electrostatic guidance. On the basis of the overall equilibrium dissociation constant of the $[ATF\text{-}2_{350–505}]_2$·$CRE_{24}$ complex (2.9×10^{-18} M^2) and the relationship $K_d = (k_{-3}/k_3)$·(k_{-4}/k_4), k_{-4} was calculated to be 0.11 s^{-1}. The concentration of ATF-$2_{350–505}$ dimer at the start of the simulation was defined by k_{-3}/k_3 or by K_{dim}. In either case, the dimer pathway could account for the observed rate of DNA binding only if the rate constant for dimerization of ATF-$2_{350–505}$ (k_3) were more than 30 times greater than the value inferred from experiment. By contrast, simulation of binding along the monomer pathway, using rate constants consistent with the overall equilibrium dissociation constant and the estimated DNA affinity of a bZIP monomer (20), reproduced the experimental results (Fig. 2*C*). The values of $k_1 = 7.5 \times 10^6$ M^{-1}·s^{-1}, $k_{-1} = 200$ s^{-1}, $k_2 = 1 \times 10^{10}$ M^{-1}·s^{-1}, and $k_{-2} = 0.0011$ s^{-1} do not represent a unique solution: a range of reasonable rates allowed the experimental data to be simulated under the monomer pathway. Like simpler bZIP peptide models, we propose that ATF-$2_{350–505}$ follows the monomer pathway to bind specific DNA.

The bHLHZip Protein Max Follows the Monomer Pathway to Bind DNA. We performed an analogous set of experiments with the bHLHZip protein Max (21) to examine whether a protein possessing a more globular dimerization domain also preferred the monomer pathway. The CD spectrum of $Max_{22–113}$ was consistent with a fully helical dimerization domain at concentrations greater than 10 μM. At lower concentrations, the $Max_{22–113}$ dimer dissociated into unstructured monomers (K_{dim} = 0.6 μM) (22, 23) that were detected by an increase in ellipticity at 222 nm (Fig. 3*A*).

The kinetics of the $Max_{22–113}$ monomer–dimer transition were monitored using CD and fluorescence polarization spectroscopy. The $Max_{22–113}$ dimer was formed at concentrations above 5 μM, diluted rapidly, and the ellipticity at 222 nm or the extent of fluorescence polarization was monitored. Initial fluorescence polarization experiments (24) using a fluorescein-labeled Max derivative, $Max^{SFlu}_{22–105}$, indicated that relaxation was slow ($1/\tau < 0.002$ s^{-1}; Fig. 3*B Inset*). A precise relaxation rate

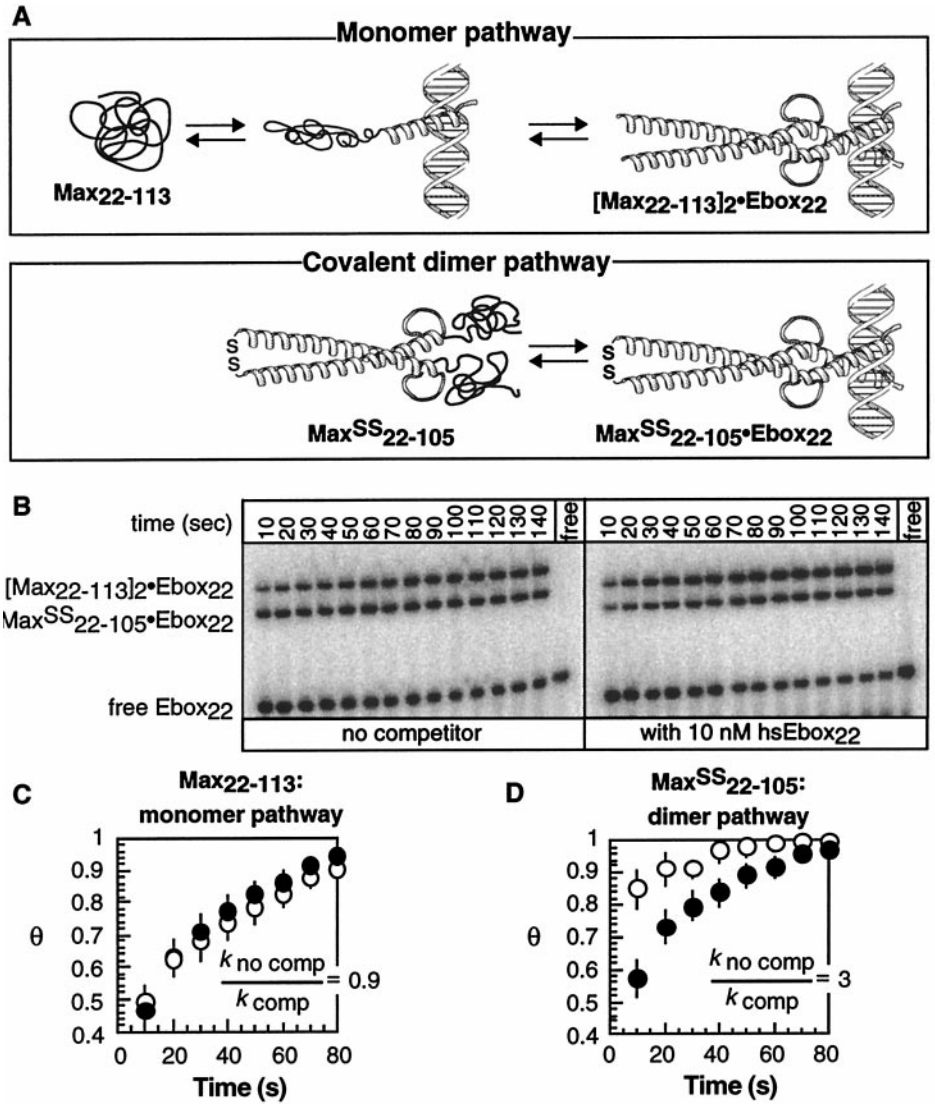

Fig. 4. Comparison of the rate of DNA binding through the monomer and dimer pathways in the presence and absence of excess nonspecific competitor DNA. (*A*) Scheme illustrating the monomer-binding pathway utilized by $Max_{22–113}$ and the covalent dimer pathway utilized by $Max^{SS}_{22–105}$. (*B*) Phosphorimage illustrating the relative rate of [^{32}P]$Ebox_{22}$ binding by $Max_{22–113}$ and $Max^{SS}_{22–105}$ in the presence or absence of competitor $hsEbox_{22}$. The fraction of DNA bound (Θ) by either $Max_{22–113}$ (*C*) or $Max^{SS}_{22–105}$ (*D*) at each time point in the absence (○) or presence (●) of $hsEbox_{22}$ DNA was normalized to a value of $\Theta = 1$ at equilibrium and fit to a single exponential to give values of $k_{no\ comp}$ and k_{comp}, respectively. Each point represented the average of at least four independent experiments. Error bars represent SE.

of $1/\tau = 0.0013 \pm 0.0001\ s^{-1}$ was determined by CD (Fig. 3*B*). This value, in combination with the independently measured equilibrium dissociation constant of the $Max_{22–113}$ dimer (0.6 μM), indicated that the $Max_{22–113}$ dimer formed slowly ($k_3 = 700\ M^{-1}\ s^{-1}$) and was kinetically stable ($k_{-3} = 0.00044\ s^{-1}$).

To evaluate whether the $Max_{22–113}$ dimer could function as an intermediate during formation of the specific DNA complex, we monitored association of $Max_{22–113}$ with ^{32}P end-labeled $Ebox_{22}$ ([^{32}P]$Ebox_{22}$) by gel electrophoresis (Fig. 3*C*). $Max_{22–113}$ bound [^{32}P]$Ebox_{22}$ rapidly at all concentrations tested, with half-lives between 25 (2 nM $Max_{22–113}$) and 60 (0.75 nM $Max_{22–113}$) sec.

Formation of the $[Max_{22–113}]_2$·$Ebox_{22}$ complex along the monomer and dimer pathways was simulated by using numerical integration (15) (Fig. 3*C*). For simulation of the dimer pathway, we employed experimentally determined values for k_3 (700 M^{-1}·s^{-1}) and k_{-3} (0.00044 s^{-1}); k_4 was set at $10^{10}\ M^{-1}$·s^{-1}, the largest allowed second-order rate constant (19) and k_{-4} was defined to be $0.016\ s^{-1}$ so that the overall equilibrium dissociation constant calculated from the rates matched the experimentally determined equilibrium dissociation constant of the complex ($10^{-18}\ M^2$). This simulation indicated that, along the dimer pathway, 7,000 sec were required for association of 2 nM $Max_{22–113}$ with one-half of the available 50 pM $Ebox_{22}$ (Fig. 3*C*). This length of time was at least 150 times longer than the experimentally determined half-life at this concentration (25 sec) (Fig. 3*C*). By contrast, simulation of $Ebox_{22}$ binding along the monomer pathway using rate constants ($k_1 = 8 \times 10^7\ M^{-1}$·$s^{-1}$, $k_{-1} = 80\ s^{-1}$, $k_2 = 8 \times 10^9\ M^{-1}$·$s^{-1}$, and $k_{-2} = 0.008\ s^{-1}$) that were physically reasonable and consistent with the overall equilibrium dissociation constant reproduced the experimental results. These simulations indicate that the monomer pathway provides rapid access to the $[Max_{22–113}]_2$·$Ebox_{22}$ complex whereas the dimer pathway does not (Fig. 3*C*).

Why Is the Monomer Pathway Preferred? The results described above indicate that the monomer pathway is favored by bZIP and bHLHZip proteins *in vitro*. We proposed a physical explanation for the dominance of the monomer pathway based on electro-

static guidance (25–27) in an early stage of the reaction (4). Both the first and the second steps in the monomer pathway are promoted by strong electrostatic interactions, with slow formation of the dimer occurring as an isomerization on the DNA. But what benefit might the monomer pathway provide *in vivo*? Together, the monomer and dimer pathways constitute a thermodynamic cycle, and no gain in equilibrium specificity can result from partitioning along the two pathways (4). However, the two pathways proceed through different intermediates, which could interact at different rates with nonspecific proteins and DNA. Therefore, the monomer and dimer pathways could generate unequal levels of specificity prior to equilibrium. The rate at which the protein searches for and locates its specific site in the more elaborate cellular milieu will depend on the relative rates of interaction with specific and nonspecific competitors.

To compare the rates at which a protein locates its specific site via the monomer and dimer pathways, we prepared a variant of Max ($Max^{SS}_{22–105}$) that allowed us to observe DNA binding along the dimer pathway that we propose is not normally utilized (Fig. 4*A*). By virtue of a disulfide bond covalently linking the coiled coil, $Max^{SS}_{22–105}$ bypassed the slow, initial step along the dimer pathway (Fig. 4*A*). We then compared the rates with which $Max^{SS}_{22–105}$ and $Max_{22–113}$ bound [^{32}P]$Ebox_{22}$ in the presence and absence of competitor DNA containing two mutations within the 6-bp Ebox site ($hsEbox_{22}$). The fraction of [^{32}P]$Ebox_{22}$ bound (Θ) as a function of time by either $Max_{22–113}$ (Fig. 4*C*) or $Max^{SS}_{22–105}$ (Fig. 4*D*) in the absence or presence of 10 nM competitor $hsEbox_{22}$ was normalized to a value of $\Theta = 1$ at equilibrium and fit to single exponentials to give $k_{no\ comp}$ and k_{comp}, respectively. In the absence of $hsEbox_{22}$ competitor, binding of [^{32}P]$Ebox_{22}$ by $Max_{22–113}$ (Fig. 3*C*) through the two-step monomer pathway competed well with one-step binding by the constitutive dimer $Max^{SS}_{22–105}$ (Fig. 3*D*). The presence of $hsEbox_{22}$ caused the preformed dimer, $Max^{SS}_{22–105}$, to bind [^{32}P]$Ebox_{22}$ more slowly (Fig. 4*D*), whereas no effect was observed on the rate of binding by the $Max_{22–113}$ monomer (Fig. 4*C*). Similar results were obtained for competition with calf thymus DNA or with HeLa cell nuclear extracts (data not shown). Even low concentrations of nonspecific proteins and DNA selectively decreased the rate of specific complex formation by a transcription factor that followed the dimer pathway. No decrease was observed for a protein that followed the monomer pathway. The dimer pathway was slowed, presumably by formation of long-lived but nonproductive intermediates—those between the preformed dimer and nonspecific protein and DNA partners.

Implications for Transcription. *In vivo*, the mass action of excess nonspecific DNA in the nucleus favors formation of nonspecific protein–DNA complexes (2). The relatively long lifetime of a nonspecific complex containing a transcription factor dimer decreases the efficiency with which the preformed dimer locates its specific site and increases the possibility of an inappropriate transcriptional response. Binding through the monomer pathway allows a dimeric transcription factor to respond rapidly to stimuli and to locate its target site quickly without becoming entrapped kinetically at a nonspecific site (28). This method of kinetic discrimination is reminiscent of the immunological phenomenon of T cell activation (29). In the immune response, an antigen may be converted from an agonist to an antagonist by increasing the rate of dissociation from a T cell receptor. It has been suggested that coreceptor proteins slow the ligand dissociation rate and thereby stimulate T cell activation (29, 30). In the realm of transcription, a large number of viral accessory proteins, including HTLV-I Tax (31–33) and hepatitis B virus pX (34), interact with bZIP proteins and deregulate cellular transcription. The mechanism of action of these viral accessory proteins may involve decreasing the dissociation rate of bZIP proteins from nonspecific DNA as well as stabilizing bZIP dimers, which possess a less efficient search mechanism than bZIP monomers.

Note Added in Proof. Rentzeperis *et al*. (35) reported that the Arc repressor also binds DNA by following the monomer pathway.

J.J.K. and S.J.M. thank the National Science Foundation and the Organic Chemistry division of the ACS, respectively, for predoctoral fellowships. We are grateful to Stephen Burley (Rockefeller University) for clones encoding $Max_{22–113}$ and $Max^{SH}_{22–105}$, to James Hoeffler (University of Colorado, Health Science Center) for the clone encoding ATF-$2_{350–505}$, and to Hays S. Rye (Department of Genetics, Yale University School of Medicine) for assistance acquiring fluorescence polarization data. This work was supported by the National Institutes of Health.

1. Tjian, R. & Maniatis, T. (1994) *Cell* **77,** 5–8.
2. Bray, D. & Lay, S. (1997) *Proc. Natl. Acad. Sci. USA* **94,** 13493–13498.
3. Kim, B. & Little, J. W. (1992) *Science* **255,** 203–206.
4. Metallo, S. J. & Schepartz, A. (1997) *Nat. Struct. Biol.* **4,** 115–117.
5. Berger, C., Piubelli, L., Haditsch, U. & Bosshard, H. R. (1998) *FEBS Lett.* **425,** 14–18.
6. Wu, X., Spiro, C., Owen, W. G. & McMurray, C. (1998) *J. Biol. Chem.* **273,** 20820–20827.
7. Wendt, H., Thomas, R. M. & Ellenberger, T. (1998) *J. Biol. Chem.* **273,** 5735–5743.
8. Rastinejad, F., Perlmann, T., Evans, R. M. & Sigler, P. B. (1995) *Nature (London)* **375,** 203–211.
9. Holmbeck, S. M. A., Dyson, H. J. & Wright, P. E. (1998) *J. Mol. Biol.* **284,** 533–539.
10. Meinke, G. & Sigler, P. B. (1999) *Nat. Struct. Biol.* **6,** 471–477.
11. Hoeffler, J. P., Meyer, T. E., Yun, Y., Jameson, J. L. & Habener, J. F. (1988) *Science* **242,** 1430–1433.
12. Ferre-D'Amare, A. R., Prendergast, G. C., Ziff, E. B. & Burley, S. K. (1993) *Nature (London)* **363,** 38–45.
13. Zitzewitz, J. A., Bilsel, O., Luo, J., Jones, B. E. & Matthews, C. R. (1995) *Biochemistry* **34,** 12812–12819.
14. Bernasconi, C. F. (1976) *Relaxation Kinetics* (Academic, New York).
15. Barshop, B. A., Wrenn, R. F. & Frieden, C. (1983) *Anal. Biochem.* **130,** 134–145.
16. Gill, G. & Tjian, R. (1991) *Cell* **65,** 333–340.
17. Harrison, S. C. (1991) *Nature (London)* **353,** 715–719.
18. Hai, T. W., Liu, F., Allegretto, E. A., Karin, M. & Green, M. R. (1988) *Genes Dev.* **2,** 1216–1226.
19. von Hippel, P. H. & Berg, O. G. (1989) *J. Biol. Chem.* **264,** 675–678.
20. Zondlo, N. J. & Schepartz, A. (1999) *J. Am. Chem. Soc.* **121,** 6938–6939.
21. Blackwood, E. M. & Eisenman, R. N. (1991) *Science* **251,** 1211–1217.
22. Fairman, R., Bernan-Steed, R. K., Anthony-Cahill, S. J., Lear, J. D., Stafford, W. F., DeGrado, W. F., Benfield, P. A. & Brenner, S. L. (1993) *Proc. Natl. Acad. Sci. USA* **90,** 10429–10433.
23. Horiuchi, M., Kurihara, Y., Katahira, M., Maeda, T., Saito, T. & Uesugi, S. (1997) *J. Biochem. (Tokyo)* **122,** 711–716.
24. James, B. R. & Williams, R. J. P. (1961) *J. Chem. Soc.* 2007–2019.
25. Schreiber, G. & Fersht, A. R. (1996) *Nat. Struct. Biol.* **3,** 427–431.
26. Getzoff, E. D., Tainer, J. A., Weiner, P. K., Kollman, P. A., Richardson, J. S. & Richardson, D. C. (1983) *Nature (London)* **306,** 287–290.
27. Getzoff, E. D., Cabelli, D. E., Fisher, C. L., Parge, H. E., Viezzoli, M. S., Banci, L. & Hallewell, R. A. (1992) *Nature (London)* **358,** 347–351.
28. Pomerantz, J. L., Wolfe, S. A. & Pabo, C. O. (1998) *Biochemistry* **37,** 965–970.
29. Rabinowitz, J. D., Beeson, C., Lyons, D. S., Davis, M. M. & McConnell, H. M. (1996) *Proc. Natl. Acad. Sci. USA* **93,** 1401–1405.
30. Vignali, D. A. A. & Strominger, J. L. (1994) *J. Exp. Med.* **179,** 1945–1956.
31. Perini, G., Wagner, S. & Green, M. R. (1995) *Nature (London)* **376,** 602–605.
32. Baranger, A. M., Palmer, C. R., Hamm, M. K., Giebler, H. A., Brauweiler, A., Nyborg, J. K. & Schepartz, A. (1995) *Nature (London)* **376,** 606–608.
33. Wagner, S. & Green, M. R. (1993) *Science* **262,** 395–399.
34. Palmer, C. R., Gegnas, L. D. & Schepartz, A. (1997) *Biochemistry* **36,** 15349–15355.
35. Rentzeperis, D., Jonsson, T. & Sauer, R. T. (1999) *Nat. Struct. Biol.* **6,** 569–573.